Materials Today Energy 5 (2017) 66–71

Contents lists available at ScienceDirect

Materials Today Energy

journal homepage: www.journals.elsevier.com/materials-today-energy/

Improvement of both efficiency and stability in organic photovoltaics by using water-soluble anionic conjugated polyelectrolyte interlayer

Kyung-Geun Lim [a], Mi-Ri Choi [a], Tae-Woo Lee [b, *]

[a] Department of Materials Science and Engineering, Pohang University of Science and Technology (POSTECH), 77 Cheongam-Ro, Nam-Gu, Pohang, Gyungbuk 37673, Republic of Korea
[b] Department of Materials Science and Engineering, Seoul National University (SNU), 1 Gwanak-ro, Gwanak-gu, Seoul 08826, Republic of Korea

ARTICLE INFO

Article history:
Received 25 January 2017
Received in revised form
27 March 2017
Accepted 29 April 2017
Available online 16 May 2017

Keywords:
Electron transport
Interface dipole
Lifetime
Organic photovoltaic

Although the prominent progress of the conjugated polyelectrolytes (CPEs) in organic photovoltaics (OPVs), the reliability of the device with CPEs was not mainly focused up to date and furthermore the principle of interfacial dipole moment μ_{ID} and corresponding energy level alignment in the device with a CPE interlayer were not clearly understood to explain the improved power conversion efficiency *PCE*. We report a water-soluble CPE, poly(2,5-bis(3-sulfonatopropoxy)-1,4-phenylene, disodium salt-*alt*-1,4-phenylene) (PPP-OPSO$_3$) interlayer that increases both the device lifetime under continuous irradiation and *PCE* of OPVs. The μ_{ID} of a PPP-OPSO$_3$ interlayer that is in intimate contact with adjacent layers can be increased by nano-morphological control; as a result, the built-in potential and device characteristics are significantly enhanced. We investigated the mechanism by which the PPP-OPSO$_3$ morphology affected of energetic alignment and enhanced characteristics. The PPP-OPSO$_3$ interlayer greatly increased the *PCE* to 6.7%, which is significantly greater than in the device with Al (5.0%) and increased half-life time LT_{50} under continuous simulated solar irradiation by 2.7 times despite the solution processing of water-dissolved PPP-OPSO$_3$.

* Corresponding author.
E-mail address: twlees@snu.ac.kr (T.-W. Lee).

http://dx.doi.org/10.1016/j.mtener.2017.04.005

1. Introduction

Organic photovoltaics (OPVs) have advantages such as flexibility, low cost, and simple solution-process fabrication. However OPVs have insufficient power conversion efficiency *PCE* and half-life time LT_{50}; these demerits must be solved for commercialization. Methods to achieve OPVs that have high *PCE* and long LT_{50} have been used such as controlling the morphology of the active layer [1–5], synthesizing photoactive materials with low bandgap or high transport mobility [6–12], and employing interlayers between the photoactive layer and electrodes [13–17].

Various kinds of interlayers can affect the *PCE* and LT_{50} critically and simultaneously. To introduce an efficient interlayer between the active layer and the negative electrode, vacuum-processed metal compounds (e.g., LiF, BaF_2) and low-work-function metals (e.g., Ca, Ba) have been used to reduce the interfacial energy barrier of an Al top electrode [18–23]. Furthermore, recent research into solution-processed negative electrode interlayers that uses an orthogonal solvent that does not dissolve the photoactive layer have conducted to improve performance and reliability in the device using low-cost non-vacuum fabrication processes [24–31].

A cathode interlayer has been used to improve the *PCE* of OPVs. Materials used for solution-processing fabrication include insulating dipole polymers [26,30] and conjugated polyelectrolytes (CPEs) [31–49]. However, the LT_{50} under continuous illumination has not been mainly investigated for devices that have a solution-processed negative electrode interlayer, although the device reliability is critically important to commercialize the OPVs. In addition, the mechanism by which the dipole polymers build the actual dipole moment at the interface has not been investigated clearly to understand and improve the device characteristics.

In this study, we used an ultrathin water-soluble CPE interlayer of poly(2,5-bis(3-sulfonatopropoxy)-1,4-phenylene, disodium salt-*alt*-1,4-phenylene) (PPP-OPSO$_3$) [50,51] to achieve highly efficient and reliable OPVs, and investigated the interfacial dipole moment that originated from the distribution of ionic moieties at the interface between adjacent layers. We studied how orientation of the ionic moiety and nano-morphological control of CPE layer affected dipole moment alignment to decrease the interfacial

energy barrier. The device with the PPP-OPSO$_3$ interlayer had improved open circuit voltage V_{oc}, short circuit current J_{sc}, fill factor *FF* and *PCE*, and significantly extended device reliability under continuous simulated solar irradiation.

2. Results and discussion

We used a water-soluble CPE, PPP-OPSO$_3$, as the multifunctional ultrathin interlayer for the solution processed OPVs (Fig. 1). We investigated the photovoltaic characteristics of poly(3-hexylthiophene) (P3HT) [6,6]:-phenyl C60-butyric acid methyl ester) (PC$_{60}$BM) and poly[N-9″-heptadecanyl-2,7-carbazole-alt-5,5-(4′,7'-di-2-thienyl-2′,1′,3'-benzothiadiazole) (PCDTBT) [6,6]:-phenyl C70-butyric acid methyl ester) (PC$_{70}$BM) devices with PPP-OPSO$_3$ interlayer. We used PCDTBT as low bandgap and deep HOMO photoactive materials to show the universality of PPP-OPSO$_3$ interlayer and a potential for better device efficiency. To amplify the effect of the PPP-OPSO$_3$ interfacial layer on the device characteristics, a self-organized hole extraction layer (SOHEL) [52,53] based on poly(3,4-ethylenedioxythiophene):poly(4-styrenesulfonate) (PEDOT:PSS) and a perfluorinated ionomer (PFI) was used as the hole extraction layer to achieve Ohmic contact with the deep HOMO level of the donor material, PCDTBT. An ultrathin PPP-OPSO$_3$ interfacial layer was cast by spin-coating of water-dissolved PPP-OPSO$_3$ solution on top of photoactive layers. We also used a conventional vacuum-deposited interfacial layer (LiF or Ca) to compare the device characteristics of the OPVs with PPP-OPSO$_3$ interlayer.

The current density-voltage (*J-V*) characteristics of the P3HT:PC$_{60}$BM and PCDTBT:PC$_{70}$BM devices with PPP-OPSO$_3$ interlayer were obtained under irradiation of air mass (AM)-1.5 global simulated sunlight at an intensity of 100 mW cm^{-2} (Fig. 2a, c). The PPP-OPSO$_3$ interlayer improved the performance parameters of OPVs compared with the Al only and other interlayers (Tables 1 and 2). V_{oc} of the devices with a 3.5-nm-thick PPP-OPSO$_3$ interlayer were 0.55 V for P3HT:PC$_{60}$BM and 0.89 V for PCDTBT:PC$_{70}$BM, which were significantly increased compared with that with Al only (0.44 V for P3HT:PC$_{60}$BM and 0.81 V for PCDTBT:PC$_{70}$BM). Moreover, *FF* of the devices with PPP-OPSO$_3$ interlayer were increased (62.6% for P3HT:PC$_{60}$BM and 62.3% for PCDTBT:PC$_{70}$BM) compared with the Al only (48.7% for P3HT:PC$_{60}$BM and 51.9% for PCDTBT:PC$_{70}$BM) due to the increased shunt resistance R_{shunt} (from 230 to 340 Ω cm^2 for P3HT:PC$_{60}$BM device and from 366.0 to 572.4 Ω cm^2 for PCDTBT:PC$_{70}$BM device) and decreased series resistance R_{series} (from 13.3 to 6.5 Ω cm^2 for P3HT:PC$_{60}$BM device and from 16.4 to 6.6 Ω cm^2 for PCDTBT:PC$_{70}$BM device). *Jsc* of the PCDTBT:PC$_{70}$BM devices showed very slight changes depending on interlayers as the comparable EQE results regardless of interlayers

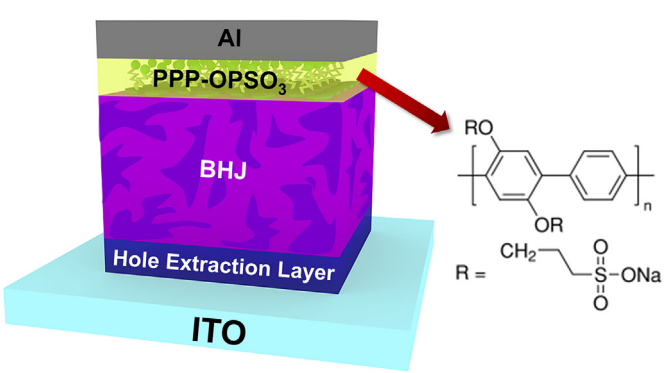

Fig. 1. Architecture of OPV device with PPP-OPSO$_3$ interlayer and its chemical structure.

(Figure S1). Therefore, the corresponding *PCE* of the devices were improved to 3.8% for P3HT:PC$_{60}$BM and 6.7% for PCDTBT:PC$_{70}$BM compared to the devices without the interlayer (2.1% and 5.0%, respectively). The *PCEs* of PPP-OPSO$_3$/Al devices are higher than even that of LiF/Al and Ca/Al devices. The dark currents of the devices with PPP-OPSO$_3$/Al were increased greatly compared with Al only devices (Fig. 2b, d) because of a better electron injection at the PPP-OPSO$_3$/Al interface than Al only. The rectification ratio (forward-biased current/reverse-biased current) at 2.0 V in the dark *J–V* characteristics was ~10^3 for PCDTBT:PC$_{70}$BM/PPP-OPSO$_3$/Al device but only ~10^2 for the device without the interlayer, and the device with Ca/Al. Furthermore, *PCE* of P3HT:PC$_{60}$BM device was slightly increased in the device with 3.5-nm-thick PPP-OPSO$_3$ interlayer (3.8%) compared with that of 4.8-nm-thick (3.5%) due to the reduced R_{series} of the P3HT:PC$_{60}$BM/PPP-OPSO$_3$ device with thickness of 3.5 nm (6.5 Ω cm^2) compared to the one with thickness of 4.8 nm (8.3 Ω cm^2). It is because ionic polymers have randomly-orientated dipole moments in the ionic aggregates of the bulk film [54]. So the overall dipole moment of the thick PPP-OPSO$_3$ layer was reduced compared with the larger dipole moments at the interface with the adjacent layer of thin PPP-OPSO$_3$. Because of these so-called interfacial dipole moments μ_{ID} at the interface with adjacent layer of CPE layers, a large shift and adjustment of energy level occurred at the cathode interface and the photoactive interface [31,55,56]. As a result of the energy level shift, the energy level offset Φ at the interface was correlated with the dipole moments of interlayers with the adjacent layer as

$$\Delta\Phi = \frac{N\mu cos\theta}{\varepsilon_0 \varepsilon} \quad (1)$$

where N is the surface dipole concentration, μ is the dipole moment, θ is the angle which the dipole makes to the surface normal, ε_o is the vacuum permittivity, and ε is the static dielectric constant [57–59]. Therefore, Φ at the interface decreases linearly when the interlayer have a high surface dipole concentration, a stronger dipole moment, and a more normal angle toward the air surface of the layer.

To investigate how device characteristics were improved by the reduction in $\Delta\Phi$ at the electron extraction contact by the PPP-OPSO$_3$ interlayer, we analyzed the energy level alignment and the μ_{ID} of PPP-OPSO$_3$ interlayer (Fig. 3). We investigated the vacuum level shift ΔE_{vac} in the P3HT:PC$_{60}$BM with our PPP-OPSO$_3$ interlayer because the energy level alignment in the device originates from the energy state of adjacent layers and particularly by ΔE_{vac} at the interlayers [31,55,56]. The secondary cut-off of P3HT:PC$_{60}$BM thin film (17.26 eV) on the high binding energy state of ultraviolet photoelectron spectroscopy (UPS) spectra was shifted to higher binding energy depending on thickness of PPP-OPSO$_3$ interlayer (17.32 eV for 4.8 nm, 17.47 eV for 3.5 nm) (Fig. 3a). Because the alkali-metal counter-ions (Na$^+$) interact intimately with the surrounding polar solvent (water) in dilute solution, they are preferentially arranged at the air surface side of the layer, whereas the sulfonated poly(*p*-phenylene) backbones are located at the photoactive layer [31]. Therefore, μ_{ID} which originates from the interfacial polarization at the intimate contact between the dipole layer and the adjacent layers points toward the photoactive layer, and E_{vac} is shifted as depicted in Fig. 3b. The net dipole moment is determined primarily by μ_{ID} at the intimate contact between the dipole layer and the metal or photoactive layer, not by intrinsic molecular dipoles μ_{MD} [31,60]. In addition, ΔE_{vac} and resulting $\Delta\Phi$ were larger at the interface between the photoactive layer and the PPP-OPSO$_3$ interlayer with optimized thickness (3.5 nm) than at that with 4.8-nm thickness. As a result, the energy level offset at the electron extraction contact Φ_e was reduced, and the difference of

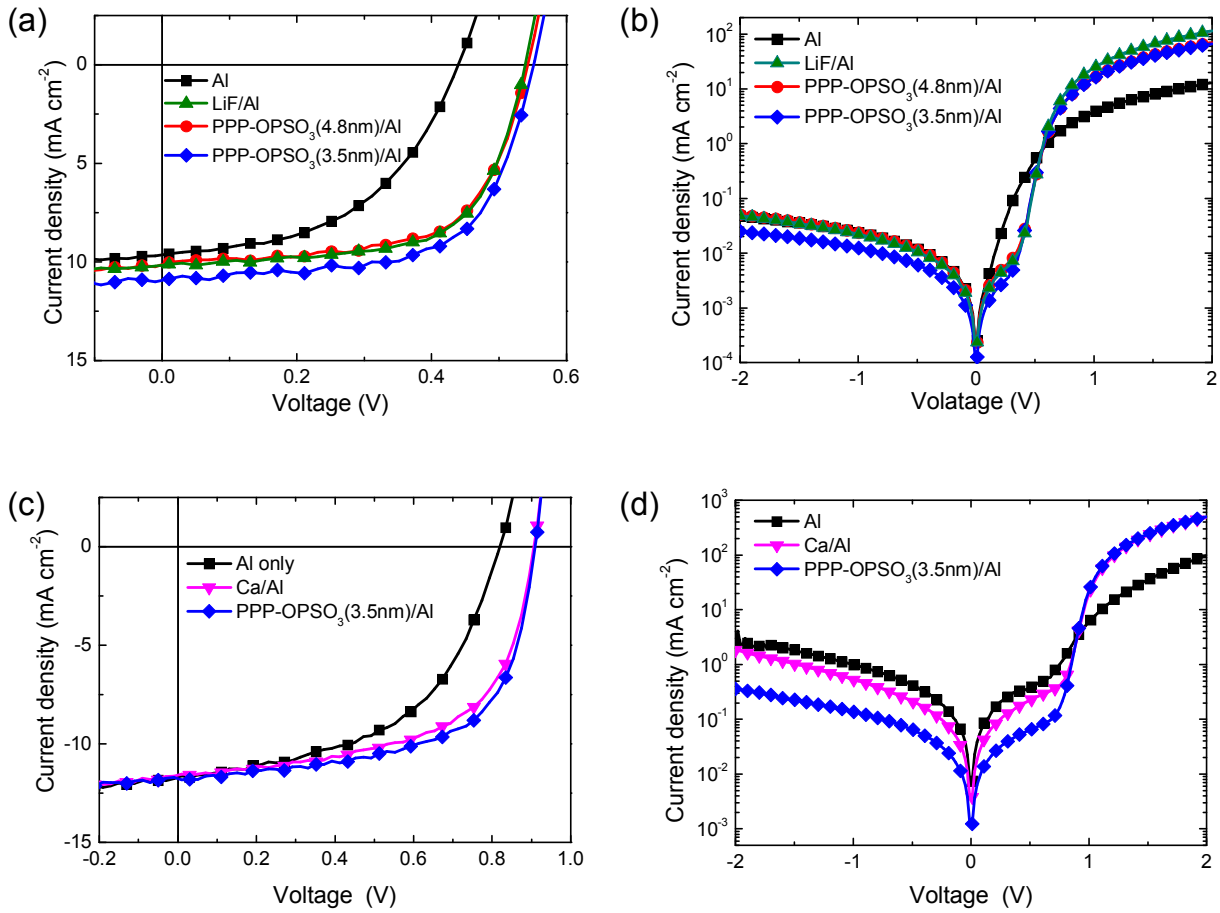

Fig. 2. Current density-voltage characteristics of the device with PPP-OPSO$_3$ interlayer for P3HT:PC$_{60}$BM device (a) at 100 mW cm^{-2}, (b) in the dark; and for PCDTBT:PC$_{70}$BM device (c) at 100 mW cm^{-2}, (d) in the dark.

Table 1
Device characteristics of P3HT:PC$_{60}$BM OPVs with PPP-OPSO$_3$ interlayers.

Cathode interlayer	V_{oc} [V]	J_{sc} [mA cm^{-2}]	*FF* [%]	*PCE* [%]	R_{shunt} [Ω cm^2]	R_{series} [Ω cm^2]
No interlayer (Al only)	0.44	9.7	48.7	2.1	230	13.3
LiF	0.53	10.2	64.9	3.5	537	7.1
PPP-OPSO$_3$ (4.8 nm)	0.54	10.2	63.2	3.5	498	8.3
PPP-OPSO$_3$ (3.3 nm)	0.55	11.0	62.6	3.8	340	6.5

Table 2
Device characteristics of PCDTBT:PC$_{70}$BM OPVs with PPP-OPSO$_3$ interlayers.

Cathode interlayer	V_{oc} [V]	J_{sc} [mA cm-2]	*FF* [%]	*PCE* [%]	R_{shunt} [Ω cm2]	R_{series} [Ω cm2]
No interlayer (Al only)	0.81	11.8	51.9	5.0	366	16.4
Ca	0.89	11.6	58.3	6.2	528	7.3
PPP-OPSO$_3$ (3.3 nm)	0.89	11.7	62.3	6.7	572	6.6

effective work function between two electrodes, so called built-in potential (V_{bi}), was increased in the device; therefore V_{oc} and *FF* were increased in the device with PPP-OPSO$_3$ interlayer as an efficient electron extraction layer [61].

We used atomic force microscopy (AFM) to investigate the surface morphology of the PPP-OPSO$_3$ layer on the on P3HT:PC$_{60}$BM photoactive layer (Fig. 4a). The PPP-OPSO$_3$ layers were deposited by spin-casting at 2000 rpm (Fig. 4b) and 4000 rpm (Fig. 4c) on bare P3HT:PC$_{60}$BM surface to control the thickness and morphology of the PPP-OPSO$_3$ layer. The layers consisted of a number of molecular grains evenly distributed on the P3HT:PC$_{60}$BM surface (Fig. 4b–c). The grain size of PPP-OPSO$_3$ layer was decreased as spin-speed increased (~30 nm for 2000 rpm and ~20 nm for 4000 rpm), because the PPP-OPSO$_3$ grains are grown by a combination of ionic interaction between the ionic groups, repulsion against the hydrophobic polymer backbones [54], and the centrifugal force during spin-casting. We also measured AFM height images of PPP-OPSO$_3$ interlayer on photoactive layer (Figure S2). When we increased the spin-speed, the ratio of the dispersion force (i.e. centrifugal force during spin-casting) over the attractive interaction between PPP-OPSO$_3$ molecules was increased, then grain size and thickness PPP-OPSO$_3$ layer were reduced. We compared ionic alignment of PPP-OPSO$_3$ interlayers depending on morphology (Figure S3). Randomly orientated ionic molecules, which is formed in bulk ionic aggregates of PPP-OPSO$_3$ interlayer with thick layer and large grains, reduce a net dipole moment of interlayer (Figure S3a). However the net dipole moment of PPP-OPSO$_3$ interlayer with thin layer and small grains is increased because it is dominated by μ_{ID} at the intimate contact between PPP-OPSO$_3$ interlayer and the metal or photoactive layer (Figure S3b). Furthermore, the direction of net dipole moment according to ΔE_{vac} (pointing toward the active layer) is determined primarily by μ_{ID} (pointing toward the active layer), not by intrinsic molecular dipoles μ_{MD} (pointing toward the metal layer) (Fig. 3b). Therefore a large ΔE_{vac} of the 3.5-nm-thick PPP-OPSO$_3$ interlayer originated from its larger dipole moment than that of 4.8-nm-thick PPP-OPSO$_3$ interlayer because the dipole molecule (sulfonated

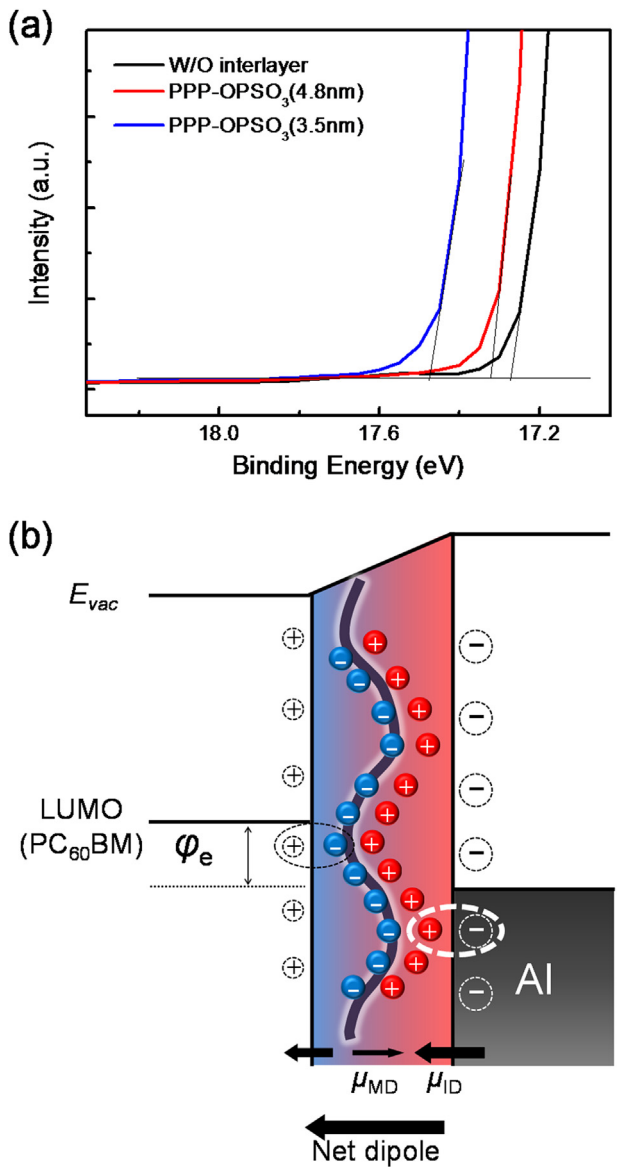

Fig. 3. Energy level analysis of PPP-OPSO$_3$ interlayer on photoactive layer. (a) UPS spectra of the P3HT:PC$_{60}$BM photoactive layer with various thickness of PPP-OPSO$_3$ interlayer; (b) Schematic energy level diagram of PPP-OPSO$_3$ interlayer on the photoactive layer surface. Interfacial dipole moment μ_{ID} at the intimate contacts of PPP-OPSO$_3$ interlayer and the resulting net dipole moment are pointing toward the active layer and thus vacuum level E_{vac} is shifted to decrease energy level offset at the electron extraction Φ_e.

poly(*p*-phenylene) backbone and alkali-metal counter ions (Na^+) was randomly orientated within the ionic aggregates in the bulk PPP-OPSO$_3$ layer. By this process, the 3.5-nm-thick PPP-OPSO$_3$ interlayer showed large $\Delta E_{vac} = 0.21$ eV and a consequent low Φ at the interface for better energy level alignment in the device.

To understand the energy level alignment and the V_{oc} increase in the device with PPP-OPSO$_3$ interlayer, we measured *C-V* characteristics of the P3HT:PC$_{60}$BM devices and PCDTBT:PC$_{70}$BM devices (Fig. 5). The capacitances of devices increased as bias voltage increased to a maximum where the voltage is called as the 'peak voltage' V_{peak}, and decreased drastically as voltage increased further; the decrease is due to recombination of majority space charges with injected opposite charges under open circuit (or flat band) condition [30]. Thus V_{peak} is correlated with V_{bi} as [21,30,62].

$$V_{bi} - V_{peak} \propto k_B T/e \quad (2)$$

where k_B is the Boltzmann constant, T is the temperature and e is the elementary charge. At room temperature, V_{peak} is always smaller than V_{bi} due to the space charges near the electrodes. Therefore, the change of V_{peak} of the device at room temperature is considered as an effective measure to estimate the change in V_{bi}. The P3HT:PC$_{60}$BM device without interlayers had $V_{peak} = 0.29$ V in the *C-V* curve, but the devices that had an LiF or PPP-OPSO$_3$ interlayer showed significantly higher $V_{peak} = 0.51$ and 0.53 V, respectively (Fig. 5a). V_{peak} of the PCDTBT:PC$_{70}$BM device with PPP-OPSO$_3$ interlayer also had higher $V_{peak} = 0.66$ V than the device with Al only (0.58 V) (Fig. 5b). The higher V_{peak} value in the device with PPP-OPSO$_3$/Al than that with Al only indicates the higher V_{bi} and corresponding V_{oc}. As a result of energetic analysis and device behavior characterization, we conclude that the device with PPP-OPSO$_3$ interlayer has lower Φ at the interface and the corresponding increased V_{bi}, thus V_{oc} increased compared with that with Al only.

We also measured LT_{50} of P3HT:PC$_{60}$BM devices with and without the PPP-OPSO$_3$ layer (Fig. 6). Device characteristics were recorded during stability measurement at intervals of 1 h under irradiance of AM-1.5 100 mW cm^{-2} light, N$_2$-filled atmosphere, and at 25.3 °C in the temperature controlled chamber until the PCE had decreased by 50%. The devices were encapsulated with a glass lid by using a UV-curable epoxy resin in a N$_2$-filled glovebox. Under continuous illumination with simulated solar light (AM 1.5G, 100 mW cm^{-2}), LT_{50} of the P3HT:PC$_{60}$BM device with PPP-OPSO$_3$ interlayers was greatly increased to 191 h (3.5-nm-thick layer) and 283 h (4.8-nm-thick layer) than that with Al only (107 h). In previous research, The P3HT:PC$_{60}$BM device with the 1-nm-thick BaF$_2$ interlayer showed a greatly (approximately nine times) increased device LT_{50} under continuous simulated solar irradiation at 100 mWcm^2 as compared with the device without an interfacial layer, despite highly hygroscopic property of metal fluoride (CsF, LiF, BaF$_2$, etc.) film. Because metal electrode diffusion into the active layer during operation is one of major causes of the OPV degradation, BaF$_2$ interlayer was used to block the diffusion of Al into the P3HT:PC$_{60}$BM layer [21]. LT_{50} was increased more in the device with 4.8-nm-thick PPP-OPSO$_3$ interlayer than 3.5 nm despite the hydrophilic nature of the PPP-OPSO$_3$ interlayer, because the PPP-OPSO$_3$ interlayer might efficiently block the atomic migration of Al layer during operation.

In addition, the device with PPP-OPSO$_3$ did not show any overshooting phenomenon of *PCE* as a function of time. During operational stability measurement, we could not observe the increase of current density at an initial stage which usually originates from ion motion of ionic interfacial polymer layer in polymer optoelectronics [63].

3. Conclusion

A water-soluble ultrathin poly(2,5-bis(3-sulfonatopropoxy)-1,4-phenylene, disodium salt-*alt*-1,4-phenylene) (PPP-OPSO$_3$) layer can increase power conversion efficiency *PCE* and half-lifetimes LT_{50} in bulk-heterojunction polymer solar cells such as poly(3-hexylthiophene) (P3HT) [6,6]:-phenyl C60-butyric acid methyl ester) (PC$_{60}$BM) and poly[N-9″-heptadecanyl-2,7-carbazole-alt-5,5-(4′,7′-di-2- thienyl-2′,1′,3′-benzothiadiazole) (PCDTBT) [6,6]:-phenyl C70-butyric acid methyl ester) (PC$_{70}$BM). We systematically investigated the mechanism of energetic alignment of PPP-OPSO$_3$ interlayer and controlled the dipole moment by adjusting the PPP-OPSO$_3$ nano-morphology. Thereby, we demonstrated that the built-in potential in the device was significantly improved depending on the interfacial dipole moment of PPP-OPSO$_3$, which was

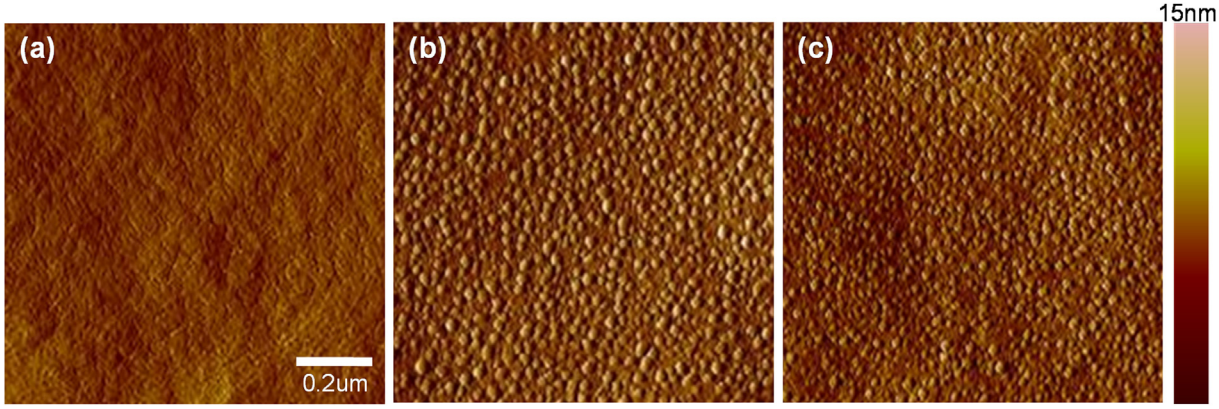

Fig. 4. AFM phase images of PPP-OPSO$_3$ interlayer atop P3HT:PC$_{60}$BM layer. (a) P3HT:PC$_{60}$BM surface; PPP-OPSO$_3$ spin-cast on P3HT:PC$_{60}$BM at (b) 2000 rpm and (c) 4000 rpm.

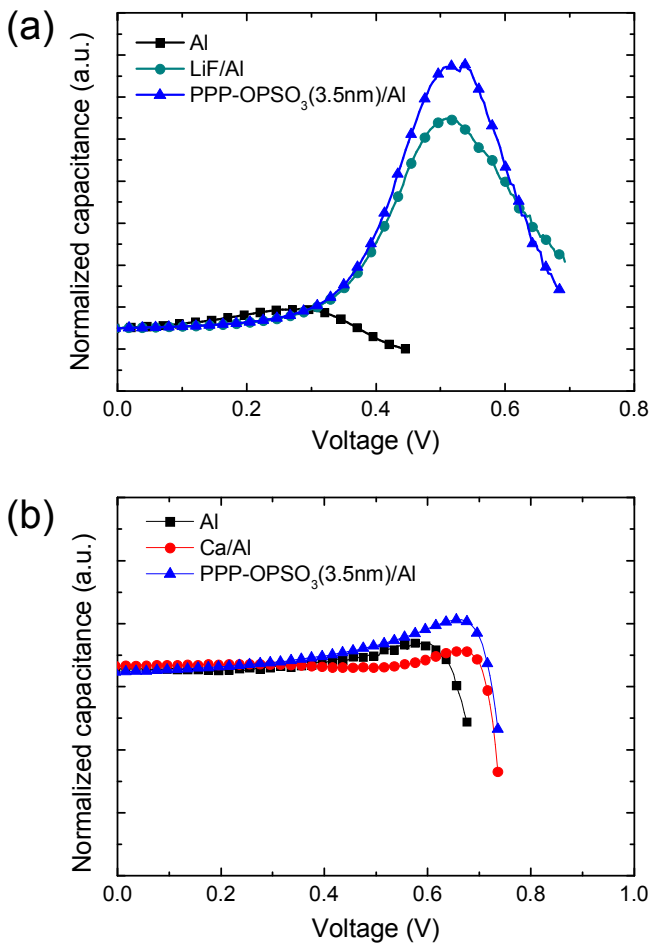

Fig. 5. Capacitance-voltage characteristics of (a) P3HT:PC$_{60}$BM device and (b) PCDTBT:PC$_{70}$BM device with PPP-OPSO$_3$ interlayer.

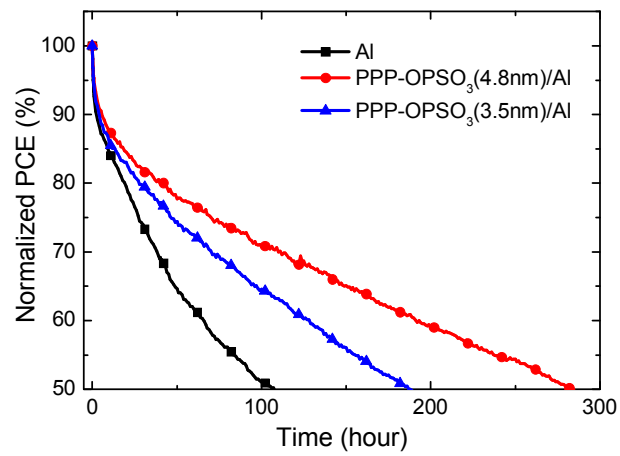

Fig. 6. PCE decay of OPVs with PPP-OPSO$_3$ interlayers of various thickness.

determined by molecular arrangement of ionic moieties at the intimate contact between the dipole layer and the metal or photoactive layer. We also demonstrated the device operational stability was also improved according to the nano-morphological effects of PPP-OPSO$_3$ interlayer. As a result, a PCDTBT:PC$_{70}$BM device with a 3.5-nm-thick PPP-OPSO$_3$ interlayer/Al showed a remarkably improved *PCE* (6.7%) compared with the device with Al only (5.0%) and a device with a conventional vacuum-processed Ca/Al interlayer (6.2%). LT_{50} also significantly increased from 107 h (without a CIL) to 283 h for the P3HT:PC$_{60}$BM device with 4.8-nm-thick PPP-OPSO$_3$ interlayer/Al.

4. Experimental section

Device Fabrication: A PEDOT:PSS layer (35 nm) was spin cast on top of a pre-patterned indium tin oxide (ITO) substrate, baked at 200 °C for 10 min, then transferred to a nitrogen glove box. The active layer of ~200 nm thickness was deposited by spin-coating P3HT:PC$_{60}$BM solution (in 1:1 wt ratio) dissolved in 1,2-dichlorobenzene. PCDTBT:PC$_{70}$BM solution (in a 1:4 wt. ratio) dissolved in 1,2-dichlorobenzene was spin-cast to form ~80-nm-thick film. To fabricate solution-processed interlayers, a solution of 1.5 mg mL^{-1} PPP-OPSO$_3$ in water was spin-coated on top of the photoactive layers to achieve different thicknesses of 4.8 nm (spin rate 2000 rpm) or 3.5 nm (4000 rpm), then dried at 50 °C for 10 min. The Ca or LiF interlayer was evaporated thermally on the photoactive layer at a deposition rate of 0.2 Å s^{-1} under a high vacuum (<5 × 10^{-7} Torr), and the Al cathode was deposited sequentially: first, 20-nm thickness at a deposition rate of 1 Å s^{-1}, then 80-nm thickness at 3 Å s^{-1} under high vacuum (<5 × 10^{-7} Torr). The photoactive area (0.06 cm^2) was defined by using metallic shadow masks. The devices were encapsulated with a glass lid by using a UV-curable epoxy resin in a N$_2$-filled glovebox.

Device Characterization: *J-V* characteristics were recorded using a computer-controlled Keithley 2400 Source Meter under

simulated AM 1.5 G irradiation at 100 mW cm^{-2} using a Xenon lamp-based solar simulator system (Newport 94043A, Class AAA, 450 W). The light intensity was calibrated to a reference solar cell (Newport 91150 V). The *C-V* characteristics were measured at 1000 Hz using a Biologic SP-300. Device lifetime was measured using a McScience Polaronix K3600 Solar Cell Reliability Test System. Device characteristics were recorded at intervals of 1 h under irradiance of AM-1.5 100 mW cm^{-2} light and N_2-filled atmosphere at 25.3 °C until the PCE had decreased by 50%.

Acknowledgements

This research was supported by the Nano Material Technology Development Program through the National Research Foundation of Korea (NRF) funded by the Ministry of Science, ICT & Future Planning (MSIP, Korea) (NRF-2014M3A7B4051747). This work was also supported by the National Research Foundation of Korea (NRF) grant funded by the Korea government (Ministry of Science, ICT & Future Planning) (NRF-2016R1A3B1908431).

Appendix A. Supplementary data

Supplementary data related to this article can be found at http://dx.doi.org/10.1016/j.mtener.2017.04.005.

References

[1] G. Li, V. Shrotriya, J. Huang, Y. Yao, T. Moriarty, K. Emery, Y. Yang, Nat. Mater 4 (2005) 864–868.
[2] V.D. Mihailetchi, H. Xie, B. de Boer, L.M. Popescu, J.C. Hummelen, P.W.M. Blom, L.J.A. Koster, Appl. Phys. Lett. 89 (2006) 012107.
[3] L.-M. Chen, Z. Hong, G. Li, Y. Yang, Adv. Mater 21 (2009) 1434–1449.
[4] J. Xue, B.P. Rand, S. Uchida, S.R. Forrest, J. Appl. Phys. 98 (2005) 124903.
[5] W.-Y. Wong, X.-Z. Wang, Z. He, A.B. Djurisic, C.-T. Yip, K.-Y. Cheung, H. Wang, C.S.K. Mak, W.-K. Chan, Nat. Mater 6 (2007) 521–527.
[6] H.-Y. Chen, J. Hou, S. Zhang, Y. Liang, G. Yang, Y. Yang, L. Yu, Y. Wu, G. Li, Nat. Photonics 3 (2009) 649–653.
[7] J. Peet, J.Y. Kim, N.E. Coates, W.L. Ma, D. Moses, A.J. Heeger, G.C. Bazan, Nat. Mater 6 (2007) 497–500.
[8] D. Mühlbacher, M. Scharber, M. Morana, Z. Zhu, D. Waller, R. Gaudiana, C. Brabec, Adv. Mater 18 (2006) 2884–2889.
[9] J.H. Hou, H.Y. Chen, S.Q. Zhang, R.I. Chen, Y. Yang, Y. Wu, G. Li, J. Am. Chem. Soc. 131 (2009) 15586–15587.
[10] S.H. Park, A. Roy, S. Beaupre, S. Cho, N. Coates, J.S. Moon, D. Moses, M. Leclerc, K. Lee, A.J. Heeger, Nat. Photonics 3 (2009) 297–302.
[11] M.-H. Chen, J. Hou, Z. Hong, G. Yang, S. Sista, L.-M. Chen, Y. Yang, Adv. Mater 21 (2009) 4238–4242.
[12] U. Mayerhöffer, K. Deing, K. Gruß, H. Braunschweig, K. Meerholz, F. Würthner, Angew. Chem. Int. Ed. 48 (2009) 8776–8779.
[13] D.Y. Kim, J. Subbiah, G. Sarasqueta, F. So, H. Ding, Irfan, Y. Gao, Appl. Phys. Lett. 95 (2009) 093304.
[14] X. Jiang, H. Xu, L. Yang, M. Shi, M. Wang, H. Chen, Sol. Energy Mater. Sol. Cells 93 (2009) 650–653.
[15] J.H. Park, T.-W. Lee, B.-D. Chin, D.H. Wang, O.O. Park, Macromol. Rapid Commun. 31 (2010) 2095–2108.
[16] R. Steim, F.R. Koglera, C.J. Brabec, J. Mater. Chem. 20 (2010) 2499–2512.
[17] S.Y. Kim, O. Kwon, T. Noh, J.-J. Park, T.-L. Choi, J.H. Park, B.D. Chin, Adv. Funct. Mater 19 (2009) 1863–1868.
[18] W.J.H. Van Gennip, J.K.J. Van Duren, P.C. Thüne, R.A.J. Janssen, J.W. Niemantsverdriet, J. Chem. Phys. 117 (2002) 5031–5035.
[19] E. Ahlswede, J. Hanisch, M. Powalla, Appl. Phys. Lett. 90 (2007) 163504.
[20] T.-W. Lee, K.-G. Lim, D.-H. Kim, Electron. Mater. Lett. 6 (2010) 41–50.
[21] K.-G. Lim, M.-R. Choi, J.-H. Kim, D.H. Kim, G.H. Jung, Y. Park, J.-L. Lee, T.-W. Lee, ChemSusChem 7 (2014) 1125–1132.
[22] K.-G. Lim, J.-M. Park, H. Mangold, F. Laquai, T.-L. Choi, T.-W. Lee, ChemSusChem 8 (2015) 337–344.
[23] D.-H. Kim, K.-G. Lim, J.H. Park, T.-W. Lee, ChemSusChem 5 (2012) 2053–2057.
[24] M.S. White, D.C. Olson, S.E. Shaheen, N. Kopidakis, D.S. Ginley, Appl. Phys. Lett. 89 (2006) 143517.
[25] J.Y. Kim, S.H. Kim, H.-H. Lee, K. Lee, W. Ma, X. Gong, A.J. Heeger, Adv. Mater 18 (2006) 572–576.
[26] F. Zhang, M. Ceder, O. Inganäs, Adv. Mater. 19 (2007) 1835–1838.
[27] S.-I. Na, S.-H. Oh, S.-S. Kim, D.-Y. Kim, Org. Electron 10 (2009) 496–500.
[28] S.-H. Oh, S.-I. Na, J. Jo, B. Lim, D. Vak, D.-Y. Kim, Adv. Funct. Mater 20 (2010) 1977–1983.
[29] A. Hayakawa, O. Yoshikawa, T. Fujieda, K. Uehara, S. Yoshikawa, Appl. Phys. Lett. 90 (2007) 163517.
[30] K.-G. Lim, M.-R. Choi, H.-B. Kim, J.H. Park, T.-W. Lee, J. Mater. Chem. 22 (2012) 25148–25153.
[31] K.-G. Lim, S.M. Park, H.Y. Woo, T.-W. Lee, ChemSusChem 8 (2015) 3062–3068.
[32] Z.C. He, C. Zhang, X.F. Xu, L.J. Zhang, L. Huang, J.W. Chen, H.B. Wu, Y. Cao, Adv. Mater 23 (2011) 3086–3089.
[33] Z. He, C. Zhong, S. Su, M. Xu, H. Wu, Y. Cao, Nat. Photonics 6 (2012) 591–595.
[34] Z. He, C. Zhong, X. Huang, W.Y. Wong, H. Wu, L. Chen, S. Su, Y. Cao, Adv. Mater 23 (2011) 4636–4643.
[35] L. Chen, C. Xie, Y. Chen, Org. Electron 14 (2013) 1551–1561.
[36] C. He, C. Zhong, H.B. Wu, R. Yang, W. Yang, F. Huang, G.C. Bazan, Y. Cao, J. Mater. Chem. 20 (2010) 2617–2622.
[37] J. Luo, H.B. Wu, C. He, A.Y. Li, W. Yang, Y. Cao, Appl. Phys. Lett. 95 (2009) 043301.
[38] T. Yang, M. Wang, C. Duan, X. Hu, L. Huang, J. Peng, F. Huang, X. Gong, Energy Environ. Sci. 5 (2012) 8208–8214.
[39] B.H. Lee, I.H. Jung, H.Y. Woo, H.-K. Shim, G. Kim, K. Lee, Adv. Funct.Mater 24 (2014) 1100–1108.
[40] S.H. Oh, S.I. Na, J. Jo, B. Lim, D. Vak, D.Y. Kim, Adv. Funct. Mater 20 (2010) 1977–1983.
[41] R. Kang, S.-H. Oh, D.-Y. Kim, ACS Appl. Mater. Interfaces 6 (2014) 6227–6236.
[42] S.-I. Na, T.-S. Kim, S.-H. Oh, J. Kim, S.-S. Kim, D.-Y. Kim, Appl. Phys. Lett. 97 (2010) 223305.
[43] J.H. Seo, T.-Q. Nguyen, J. Am. Chem. Soc. 130 (2008) 10042–10043.
[44] H. Choi, J.S. Park, E. Jeong, G.-H. Kim, B.R. Lee, S.O. Kim, M.H. Song, H.Y. Woo, J.Y. Kim, Adv. Mater 23 (2011) 2759–2763.
[45] W. Lee, H. Choi, S. Hwang, J.Y. Kim, H.Y. Woo, Chem. Eur. J. 18 (2012) 2551–2558.
[46] J. Jo, J.-R. Pouliot, D. Wynands, S.D. Collins, J.Y. Kim, T.L. Nguyen, H.Y. Woo, Y. Sun, M. Leclerc, A.J. Heeger, Adv. Mater 25 (2013) 4783–4788.
[47] K. Yao, L. Chen, Y. Chen, F. Li, P. Wang, J. Mater. Chem. 21 (2011) 13780–13784.
[48] J. Seo, A. Gutacker, Y.M. Sun, H.B. Wu, F. Huang, Y. Cao, U. Scherf, A.J. Heeger, G.C. Bazan, J. Am. Chem. Soc. 133 (2011) 8416–8419.
[49] L. Chen, C. Xie, Y. Chen, Macromolecules 47 (2014) 1623–1632.
[50] S. Kim, J. Jackiw, E. Robinson, K.S. Schanze, J.R. Reynolds, J. Baur, M.F. Rubner, D. Boils, Macromolecules 31 (1998) 964–974.
[51] H.A.A. Attar, A.P. Monkman, Phys. Rev. B 86 (2012) 235420.
[52] K.-G. Lim, H.-B. Kim, J. Jeong, H. Kim, J.Y. Kim, T.-W. Lee, Adv. Mater 26 (2014) 6461–6466.
[53] K.-G. Lim, S. Ahn, Y.-H. Kim, Y. Qi, T.-W. Lee, Energy Environ. Sci. 9 (2016) 932–939.
[54] A. Eisenberg, J.-S. Kim, Introduction to Ionomers, Wiley, New York, 1998.
[55] H. Ishii, K. Sugiyama, E. Ito, K. Seki, Adv. Mater 11 (1999) 605–625.
[56] B. de Boer, A. Hadipour, M.M. Mandoc, T. van Woudenbergh, P.W.M. Blom, Adv. Mater 17 (2005) 621–625.
[57] T.-W. Lee, J. Zaumseil, S.H. Kim, J.W.P. Hsu, Adv. Mater 16 (2004) 2040–2045.
[58] T.-W. Lee, O.O. Park, L.-M. Do, T. Zyung, T. Ahn, H.-K. Shim, J. Appl. Phys. 90 (2001) 2128–2134.
[59] C. Goh, S.R. Scully, M.D. McGehee, J. Appl. Phys. 101 (2007) 114503.
[60] H.-L. Yip, S.K. Hau, N.S. Baek, H. Ma, A.K.Y. Jen, Adv. Mater 20 (2008) 2376–2382.
[61] V.D. Mihailetchi, P.W.M. Blom, J.C. Hummelen, M.T. Rispens, J. Appl. Phys. 94 (2003) 6849–6854.
[62] S.L.M. van Mensfoort, R. Coehoorn, Phys. Rev. Lett. 100 (2008) 086802.
[63] S.-H. Oh, D. Vak, S.-I. Na, T.-W. Lee, D.-Y. Kim, Adv. Mater 20 (2008) 1624–1629.